IAEA nuclear fusion

ELM simulation experiments on Pilot-PSI using simultaneous high flux plasma and transient heat/particle source

IOP Publishing and International Atomic Energy Agency — Nuclear Fusion

Nucl. Fusion **51** (2011) 073008 (8pp) doi:10.1088/0029-5515/51/7/073008

ELM simulation experiments on Pilot-PSI using simultaneous high flux plasma and transient heat/particle source

G. De Temmerman[1], J.J. Zielinski[1], S. van Diepen[1], L. Marot[2] and M. Price[3]

[1] FOM Institute for Plasma Physics Rijnhuizen, Edisonbaan 14, 3439 MN Nieuwegein, The Netherlands
[2] Department of Physics, University of Basel, Klingelberstrasse 82, CH-4056 Basel, Switzerland
[3] EURATOM/CCFE Fusion Association, Culham Science Centre, Abingdon, UK

E-mail: g.c.temmerman@rijnhuizen.nl

Received 27 December 2010, accepted for publication 28 April 2011
Published 27 May 2011
Online at stacks.iop.org/NF/51/073008

Abstract

A new experimental setup has been developed for edge localized mode (ELM) simulation experiments with relevant steady-state plasma conditions and transient heat/particle source. The setup is based on the Pilot-PSI linear plasma device and allows the superimposition of a transient heat/particle pulse to the steady-state heat flux plasma. Energy densities as high as 1 MJ m^{-2} have been reached for a pulse duration of about 1.5 ms, and for a variety of gases (H, He, Ar). In this contribution, we report on the first experiments investigating the effect of the combined steady-state/pulsed plasma on polycrystalline tungsten targets. Under such conditions the threshold for tungsten release and surface roughening is found to be much lower than in previously reported experiments. This suggests that the combination of the high flux plasma and transient heat/particle source leads to strong synergistic effects.

(Some figures in this article are in colour only in the electronic version)

1. Introduction

Edge localized modes (ELMs) are a major concern for the lifetime of the divertor plasma-facing materials (PFMs) in ITER. The very high localized heat fluxes will lead to material erosion, melting and vaporization [1]. In addition, the repetition of such thermal shocks can lead to a degradation of the material thermo-mechanical properties. In ITER, the PFMs will be submitted to both the steady-state detached divertor plasma and the intense heat and particle fluxes during ELMs. A steady-sate heat flux of about 10 MW m^{-2} is expected at the divertor targets [2] while energy densities of up to 10 MJ m^{-2} are predicted for unmitigated type-I ELMs [3]. In parallel, strong modifications of the surface morphology can occur during bombardment by low energy plasma ions (D,T, He) such as blistering [4] or formation of helium-induced nanostructure [5]. In such a situation, the transient heat/particle pulse associated with an ELM will interact with a surface with modified properties and this might strongly affect the material damage threshold, some proofs of which have been described previously [6, 7].

Several techniques are currently being used to investigate the behaviour of materials under ITER relevant transient heat loads. Electron guns such as the JUDITH facility [8] can produce relevant energy densities and durations but lack the plasma environment. Plasma guns [9] on the other hand produce heat loads and ion energies relevant for the studies of ELM/material interactions but cannot combine it to the relevant steady-state plasma. Finally, the use of powerful lasers associated with linear plasma generators [6, 7] combines a plasma environment and transient heat fluxes. Still, the plasma conditions in those devices are quite different from those expected in ITER and the use of a laser does not allow reproducing the transient particle flux associated with an ELM.

In order to overcome those limitations and allow ELM simulation experiments with relevant steady-state plasma conditions and transient heat/particle source, a new experimental setup is being developed. The initial setup is based on the Pilot-PSI linear device, whose plasma source has been modified to be compatible with pulsed operations. This allows, for the first time, the superimposition of a transient heat/particle pulse to the steady-state heat flux plasma [10]. Energy densities as high as 1 MJ m^{-2} have been reached for a pulse duration of about 1–1.5 ms [11]. In this contribution, we report on the properties of the pulsed plasmas and on the first experiments made to investigate the effect of the combined

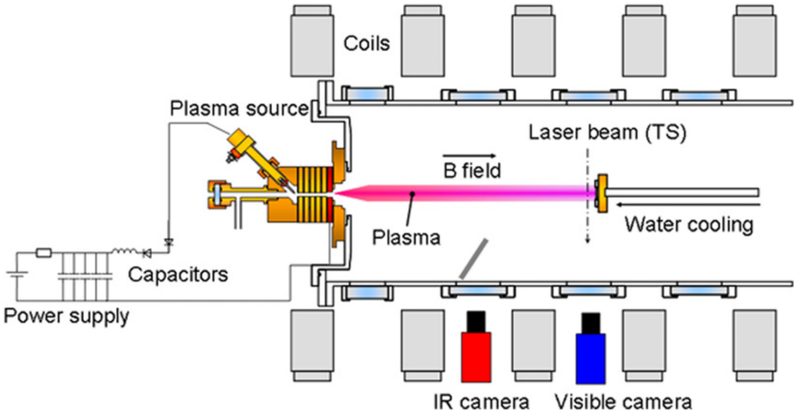

Figure 1. Schematic overview of Pilot-PSI with the pulsed source system.

steady-state/pulsed plasma on polycrystalline tungsten targets. Post-mortem analysis of the targets was performed by scanning electron microscopy (SEM). Fast visible imaging was used to determine *in situ* the threshold for tungsten release from the surface.

2. Experimental

The Pilot-PSI linear device produces plasma parameters ($n_e \sim (0.1)$–$10) \times 10^{20}\,\mathrm{m}^{-3}$, $T_e \sim 1$–$5\,\mathrm{eV}$) relevant to the study of steady-state plasma–surface interactions in the ITER divertor [12]. The high flux plasma is generated by a cascaded arc plasma source which is powered by a current regulated power supply. In parallel, a capacitor bank (8400 μF, 4.2 kJ) is connected to the plasma source and discharged in the plasma source to transiently increase the input power (figure 1). This results in a transient increase of the electron density and temperature. The plasma source was modified to accommodate the high heat fluxes generated during such pulses. Peak discharge currents of about 14 kA have been generated, corresponding to a peak input power in the plasma source of about 5.5 MW. The evolution of the discharge current and input power during a hydrogen plasma pulse is shown in figure 2. The steady-state current and voltage were 180 V and 200 A, respectively, for a magnetic field of 1.6 T and a gas flow of 10 slm (standard litres per minute). Both the current and voltage in the source increase during the plasma pulse. The peak input power in that case was about 3.8 MW. The current trace reveals a smooth bell-shaped curve, while a short spike in the source voltage can be noticed at the beginning of the pulse, which lasts for about 100 μs. A detailed study of the electrical properties of the arc during pulsed operations will be published elsewhere. The pulse duration was about 1.3 ms, although the pulse duration and shape can be adapted to the needs. The plasma source can be operated with a variety of gases (e.g. Ar, H, D, He, N) as well as with gas mixtures.

The plasma parameters are measured by means of a Thomson scattering system [13] located 17 mm in front of the plasma exposed target (figure 1). The magnetic field, the trigger to the capacitor bank and the Thomson scattering system were synchronized in time with accuracy better than 1 μs to ensure a reproducible time delay between every step of the sequence. The time evolution of the density

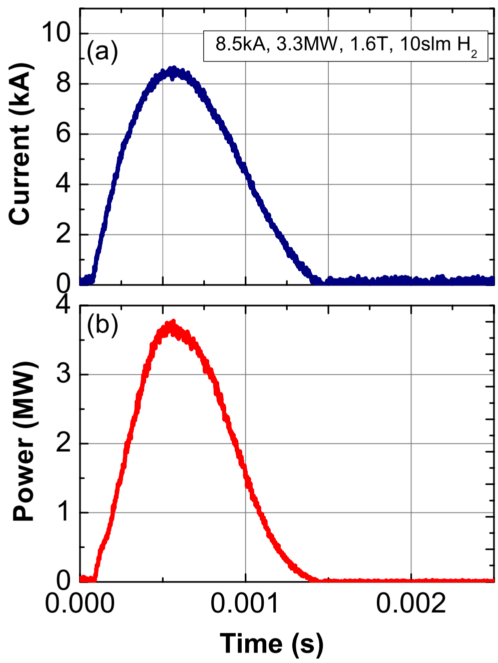

Figure 2. Temporal evolution of (*a*) the discharge current and (*b*) input power during a hydrogen plasma pulse. The peak input power was about 3.8 MW. The magnetic field was 1.6 T and the vessel pressure about 10 Pa.

and temperature during such a pulse have been described in [10, 11]. The time evolution of the surface temperature during the pulse was monitored by a fast infrared camera (FLIR SC7500MB) which measures infrared radiation in the wavelength range 2–5 μm. The frame rate of the camera was set to 10 kHz. The infrared camera was calibrated up to 3000 °C using a blackbody source. The target heat fluxes are calculated using THEODOR [14], a 2D inverse heat transfer code which considers the presence of a layer on top of the substrate. The layer is characterized with a given α parameter, the ratio of the heat conductivity to the thickness of the layer [15]. Without this parameter, negative heat fluxes can be calculated by the code because of the overestimation of the surface temperature induced by the bad thermal contact of the disturbed layer with the bulk. In order to determine the values of α to be used, the method described in [16, 17] is used, i.e. the value of α is varied until negative heat fluxes are

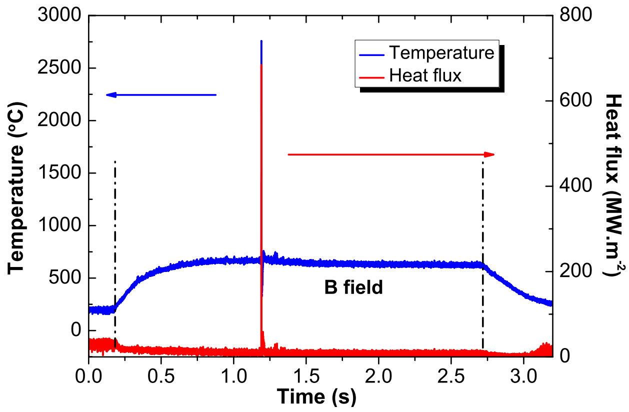

Figure 3. Temporal evolution of the surface temperature and peak heat flux of a tungsten target, illustrating the superimposition of the steady-state and pulsed plasmas.

removed. The heat fluxes derived from IR measurements have been compared with those calculated from the plasma density and temperature using sheath heat transmission factors and a relatively good agreement was found [10]. Fast visible imaging was performed using a Photron APX-RS camera equipped with interference filters (H_α at 656.2 nm, and W I at 400.9 nm) and operating at a frame rate of up to 75 kHz.

The plasma exposed target was a 30 mm diameter polycrystalline tungsten disc, 1 mm thick, which was kept at floating potential during the exposure. After polishing, the targets are ultrasonically cleaned in ethanol and acetone. They are then outgassed at 1000 °C for 15 min following a temperature ramp of 60 °C min^{-1}.

Figure 3 shows the temperature and heat flux evolution during a typical discharge. The magnetic field was triggered for a duration of 2 s, the surface temperature reached an equilibrium value (about 650 °C in the present case) after about 0.5 s. The pulsed plasma was triggered at $t = 1$ s resulting in a strong increase in the surface temperature (up to 2700 °C) during the pulse. The surface temperature then returns to its pre-pulse value.

3. Properties of the pulsed plasma

Figure 4 shows the time evolution of the H_α signal measured by the fast visible camera during a pulsed plasma compared with the time evolution of the power flux density to the target determined from infrared thermography. The temperature rise time during a pulse is in the range 0.5–1 ms which is in good agreement with typical rise times for type-I ELMs in tokamaks [3]. Evidently, the time evolution of the peak heat flux is well correlated with the time evolution of the H_α signal, which in turn is well correlated with the time evolution of the discharge current.

As described in [10, 11], the plasma parameters during a plasma pulse depend on the input power in the source, the magnetic field, the source geometry and the gas flow in the source. The plasma density increases with the input power [10], and the highest achieved plasma conditions are $n_e = 140 \times 10^{20}\,\mathrm{m}^{-3}$ and $T_e = 6$ eV. The peak heat flux to the target naturally follows the same evolutions; i.e. the higher the input power the higher the peak heat flux to the

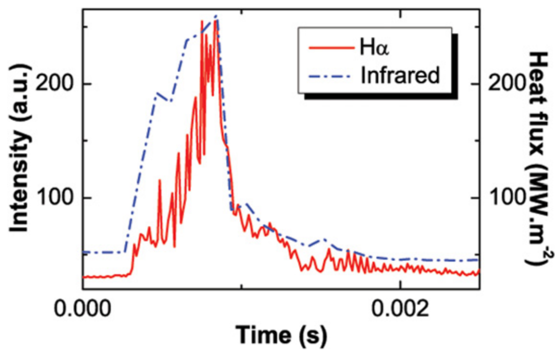

Figure 4. Temporal evolution of the H_α signal recorded by a fast filtered visible camera and the peak heat flux to the surface determined from the infrared camera.

target as illustrated by figure 5(*a*). A power scan has been performed with hydrogen, helium and argon as working gas and similar heat load levels are reached in the different cases. It should be mentioned that the conditions during the plasma pulse can be tuned independently from those during the steady-state phase, allowing a wide range of operation parameters. Figure 5(*b*) shows the peak energy density (obtained by time integration of the peak heat flux over the pulse duration) to the surface as a function of the peak input power in the plasma source. Compared with figure 5(*a*), the larger scatter observed in figure 5(*b*) is caused by slight differences in the time evolution of the peak heat fluxes for the different cases. Energy densities in the range 0.05–1 MJ m^{-2} can be achieved, which corresponds to a maximum heat flux parameter of 28 MW m^{-2} s$^{1/2}$. The use of the heat flux parameter for the comparison of the material damage threshold is justified by the fact that for short heat pulses the surface temperature increase is proportional to the product of the power density and the square root of the pulse duration.

4. Behaviour of tungsten under simultaneous steady-state/pulsed plasma exposure

4.1. Tungsten release

To study the influence of the combined steady-state/pulsed plasma on the surface damage of tungsten, tungsten targets were exposed to identical steady-state plasma conditions while the energy density deposited during the pulsed plasma was varied. The steady-state plasma duration was 2 s and the pulsed plasma was triggered at $t = 1$ s. Both hydrogen and helium plasmas were used. In that case the source settings were identical, which resulted in different surface temperatures—400 °C and 750 °C for hydrogen and helium plasmas, respectively. W I line emission at 400.9 nm was recorded by a fast visible camera, to characterize the threshold for tungsten release. The optical filter used in this study was centred around 400.5 nm and had a bandwidth of 2 nm. In order to eliminate the possible contribution of continuum emission from the plasma, the signal measured 5 cm away from the target was subtracted from the measurements. It was observed, however, that the emission from the plasma was negligible compared with the W I line intensity from the target. According to the NIST database[4], emission from iron lines

[4] http://physics.nist.gov/PhysRefData/ASD/lines_form.html

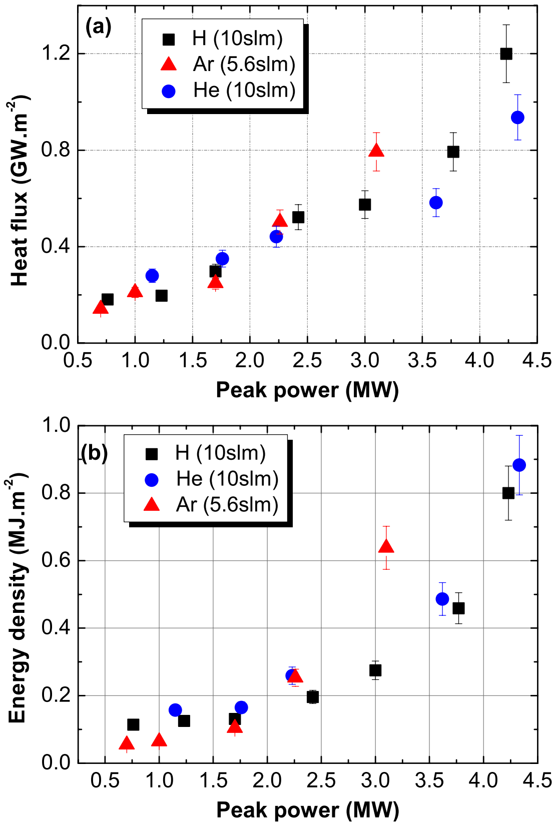

Figure 5. Evolution of (*a*) the peak heat flux to the surface and (*b*) deposited energy density as a function of the peak input power in the plasma source for different cases.

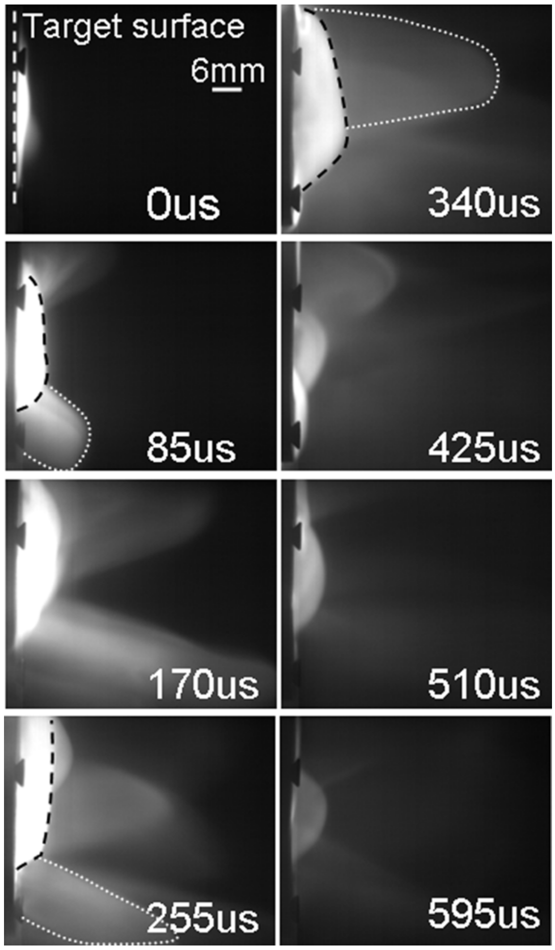

Figure 6. Series of snapshots taken by the fast visible camera (operating at 12 kHz) of the W I emission from the target during a hydrogen plasma pulse. The energy density to the target was 0.3 MJ m^{-2}.

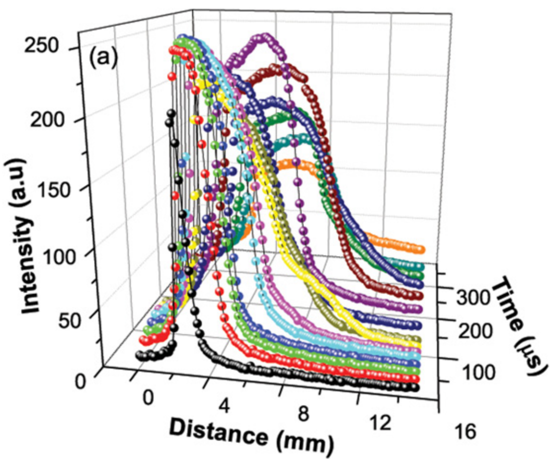

Figure 7. Time evolution of the W I line brightness profile (1D lineout) taken at the centre of the plasma exposed target during a hydrogen plasma pulse with energy density of 0.3 MJ m^{-2}.

occurs in a similar wavelength range. Although the vacuum vessel is made of stainless steel, no trace of iron has ever been found by surface analysis of the exposed samples so that the possibility of iron emission from the target is not considered.

Figure 6 shows a series of 2D snapshots from the fast filtered camera taken during a plasma pulse in hydrogen. Two main effects can be observed. First, an emission cloud is formed in front of the target (indicated by the black dashed line in figure 6). Second, extended tracks (indicated by the white dotted line in figure 6) can also be observed moving away from the target. These tracks appear quite random in nature but all appear to originate from the target. It should be mentioned that the camera was focused on the centre of the target and had a relatively narrow field of view because of the aperture used and the high magnification, this makes it difficult to assess the precise shape of these trajectories. The estimated velocity of motion of this second type of emission is in the range 50–500 m s^{-1} which is larger than the velocity of tungsten particle released from a tungsten surface during QSPA experiments [1] but in agreement with the velocity of carbon particles released during disruptions in tokamaks [18]. The precise assignment of this effect to dust particles release from the target will be investigated in future experiments.

Figure 7 shows the time evolution of the W I line brightness profile (1D lineout) taken at the centre of the plasma exposed target during a hydrogen plasma pulse similar to that of figure 6 but acquired with a frame rate of 75 kHz. A significant broadening of the emission profile is observed during the pulse and emission can be observed up to 12 mm away from the target.

A comparison of the temporal evolutions of the surface temperature (from IR imaging) and of the W I brightness is

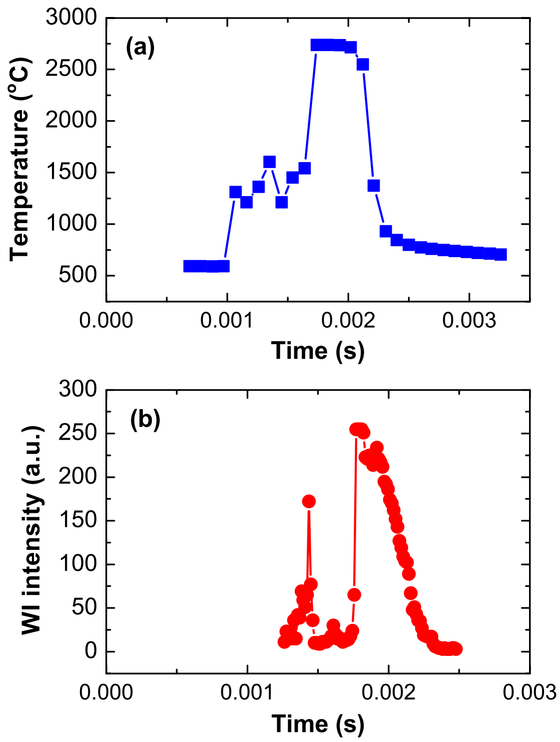

Figure 8. Time evolution of the surface temperature (*a*) and W I brightness (*b*) measured by fast infrared and visible imaging, respectively, during a hydrogen plasma pulse with energy density of $0.5\,\mathrm{MJ\,m^{-2}}$.

shown in figure 8 for a hydrogen plasma pulse with an energy density of $0.5\,\mathrm{MJ\,m^{-2}}$. The temperature rise time is about 0.7 ms in the present case. It should be mentioned here that Pilot-PSI is not equipped with a central clock system and the different fast cameras are running on their internal clock, which makes it difficult to synchronize the signals. In some cases, tungsten release from the plasma source is observed during the first $100\,\mu$s of the plasma pulse (figure 8(*b*)), although the effect is erratic in nature and not reproducible. For that reason, and since the emission from the source can clearly be distinguished from the emission from the target (different timescales), only the contribution from the target has been taken into account in the following.

Figure 9 shows the influence of the energy density to the target on the W I emission intensity, the latter was integrated over the pulse duration to account for the total release of tungsten during the pulsed plasma. For both hydrogen and helium plasma, a clear threshold behaviour is observed with no release observed below a certain energy density and increasing tungsten emission with increasing energy density after the threshold value. In the case of a hydrogen plasma, the threshold for release is around $0.2\,\mathrm{MJ\,m^{-2}}$, while no release is observed below $0.25\,\mathrm{MJ\,m^{-2}}$ for helium. The W I intensity measured during helium plasmas remains systematically lower than that measured for hydrogen plasmas. Since the electron temperature (and thus S/XB) might be different in both cases, this might contribute to the different emission intensities. It should be mentioned that no firm conclusion can be drawn on the different thresholds for helium and hydrogen because of the different surface temperatures during the steady-state phase. The evolution of the W I signal as a function of the

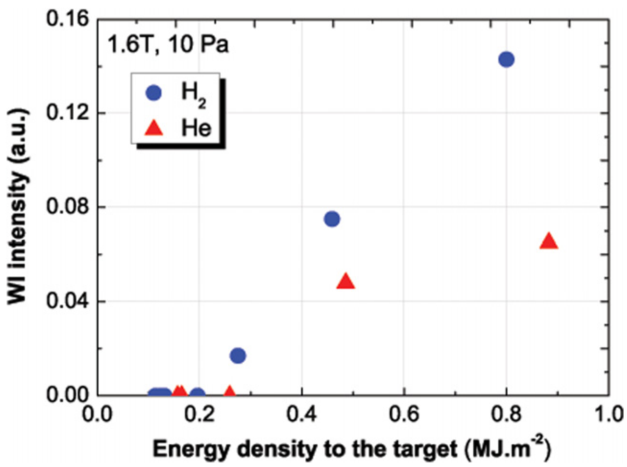

Figure 9. Evolution of the W I line intensity (integrated over the plasma pulse duration) as a function of deposited energy density for hydrogen and helium plasmas.

energy density appears to be linear, whereas an exponential increase would be expected. Although no explanation can be given yet, it is important to keep in mind that the plasma conditions during the pulse vary strongly with increasing input power and this makes the direct interpretation of the W I line intensity rather difficult. The threshold for release measured in the present experiments corresponds to a heat flux parameter of about $7\,\mathrm{MW\,m^{-2}\,s^{1/2}}$ which is much lower than the energy densities at which cracking is observed in QSPA [9] ($15\,\mathrm{MW\,m^{-2}\,s^{1/2}}$) and considerably lower than the threshold for melting ($50\,\mathrm{MW\,m^{-2}\,s^{1/2}}$).

Given that the electron temperature remains low during the plasma pulse (below 6 eV), physical sputtering of tungsten can be neglected because the ion impact energy will remain lower than the threshold for sputtering. The observed release of neutrals from the surface is probably caused by several simultaneous effects. First, during the plasma pulse, a sudden increase in the surface temperature occurs with maximum values close to the melting point for the highest energy densities so that thermal evaporation will represent an increasing particle source with increasing temperatures. Figure 10 shows the evolution of the W I brightness against the surface temperature. As mentioned above, the infrared and visible cameras are both running on their internal clocks so that the synchronization of both diagnostics is not perfect. In addition, temperature measurements on tungsten at high temperatures are complicated by the temperature-dependent emissivity. In any case, it is clear from figure 10 that the W I brightness evolves with surface temperature with a factor 10 increase in the light intensity between 1200 and 2700 °C. The tungsten release from evaporation is expected to be negligible at temperatures below 2500 °C and increases very rapidly with increasing surface temperature, which would explain the strong increase in W I intensity between 2500 and 2700 °C. However, significant emission is observed below 2200 °C. The visible camera could not be calibrated at the time of the experiments so that the tungsten release rate cannot be inferred from the measured intensity. In the future, such measurements will be repeated with synchronized cameras and calibrated visible emission diagnostics.

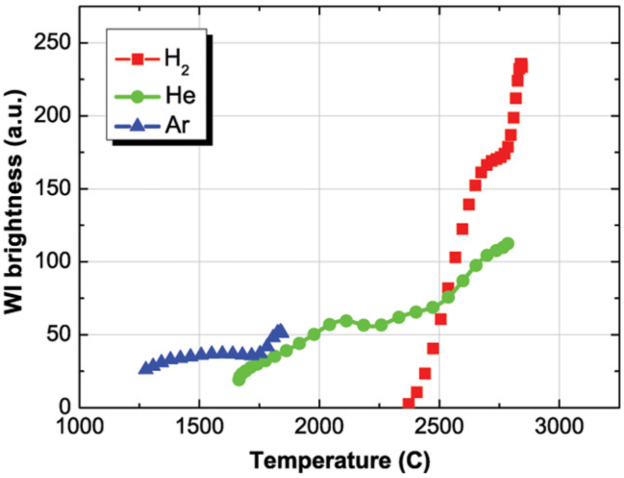

Figure 10. Evolution of the W I brightness measured by fast visible imaging as a function of the surface temperature measured by infrared thermography.

Dust release from the surface represents another possible source of tungsten and is regularly observed during experiments in the QSPA plasma gun [1], for example. Supporting this hypothesis, it has been observed that cracking of the exposed surface due to the transient heat loads could result in the formation of large particles with almost no attachment to the edges of the cracks. This effect will be described in the following section. Finally, as mentioned in [7], the blisters formed on a tungsten surface during the steady-state phase could burst during the transient heat load as a result of the sudden pressure rise. In some cases, burst blister caps were observed during the present experiments (not shown here). More experiments are ongoing to assess the influence of this effect on the global surface erosion.

4.2. Evolution of tungsten morphology

The influence of the surface morphology of tungsten surfaces exposed to combined steady-state/pulsed plasma has been investigated for hydrogen plasmas using secondary electron microscopy. Samples were exposed according to the procedure described in section 2, although in this case the steady-state plasma duration was 4 s and the plasma pulse was triggered at $t = 2$ s. The peak energy density during the pulse was 0.15 MJ m^{-2}. Since the plasma density and temperature have a Gaussian profile during the pulse [10], a gradient of energy deposition exists on the surface. Figure 11 shows the target temperature profile during the steady-state phase, with a peak temperature of about 560 °C, and during the peak of the plasma pulse when the peak surface temperature is about 1000 °C. The SEM observations were performed at the target centre corresponding to the area of maximum energy deposition and at radial positions corresponding to half the peak energy density (according to the 2D IR measurements). Samples were exposed to 10 and 17 pulses corresponding to a steady-state plasma duration of 40 s and 68 s, respectively. Reference samples were exposed to similar steady-state plasma conditions in the absence of plasma pulses to isolate the effect of the combined exposure with that of possible morphology changes induced by the hydrogen plasma alone. The plasma

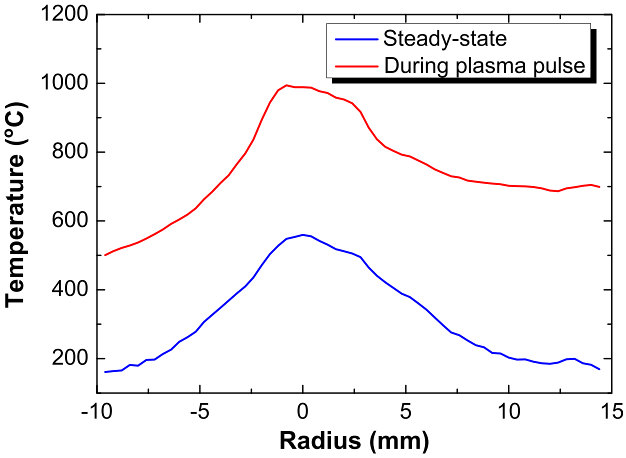

Figure 11. Surface temperature profiles measured by a fast infrared camera during the steady phase of the discharge and during the plasma pulse.

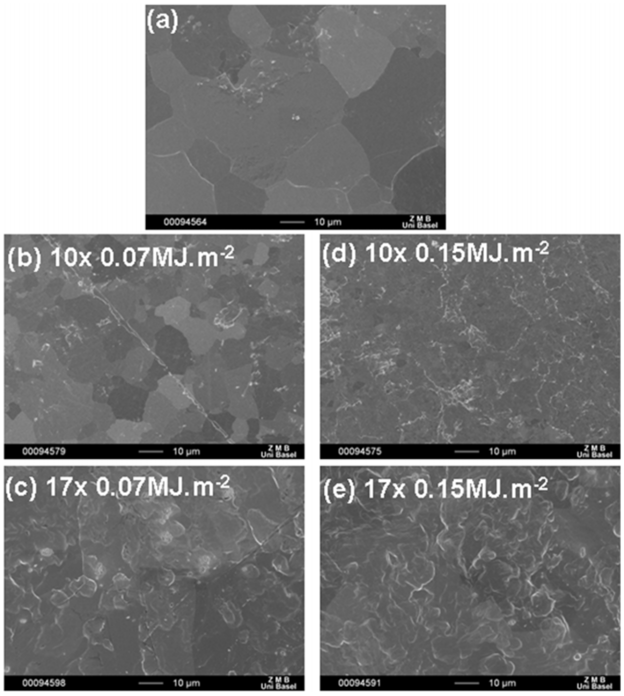

Figure 12. (*a*) SEM pictures of tungsten samples after exposure to 40 s of steady-state hydrogen plasma without plasma pulses. The following pictures show the surface morphology of tungsten targets exposed to similar steady-state plasma conditions with additional plasma pulses. (*b*) and (*c*) SEM pictures of tungsten surface after 10 and 17 plasma pulses with energy density 0.07 MJ m^{-2}, respectively. (*d*) and (*e*) Surface morphology after 10 and 17 pulses with energy density 0.15 MJ m^{-2}, respectively.

conditions during the steady-state phase were $n_e \sim 5 \times 10^{20}$ m^{-3} and $T_e \sim 1$ eV.

Figure 12(*a*) shows the morphology of the reference tungsten sample exposed for 40 s in the absence of any plasma pulse. No morphology changes can be noticed compared with that of a polished non-exposed sample. The morphology of the reference sample exposed for 68 s (not shown here) is similar to that shown in figure 12(*a*). On the other hand, significant morphology changes are observed when the surface is simultaneously subjected to plasma pulses.

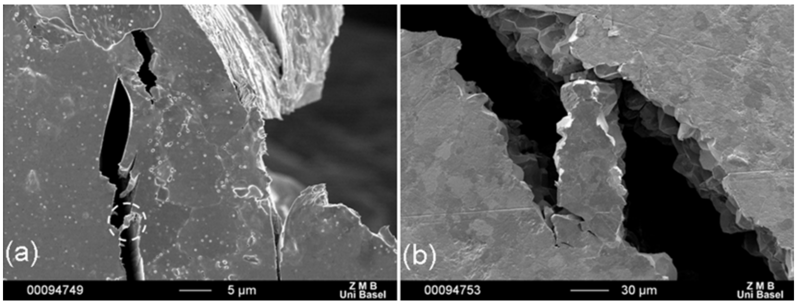

Figure 13. (*a*) and (*b*) Evidence of the formation of loosely bound particles as a result of cracking of the tungsten surface exposed to 6 pulses with energy density 0.15 MJ m^{-2} with helium as a working gas. The formation of these particles represents a possible source of dust release from the surface.

Surface roughening is already noticeable after 10 pulses at 0.07 MJ m^{-2} (figure 12(*b*)), and increases with the pulse number (figure 12(*c*)). For higher energy densities the effect is much more pronounced as illustrated by figure 12(*d*) and also evolves rapidly with the number of pulses (figure 12(*e*)).

In addition to the above mentioned surface roughening, cracking of the tungsten surface is also observed. More importantly, the formation of dust-like particles is regularly observed at the surface of the cracks; examples of such an effect are shown in figure 13. The size of those particles can be between a few micrometres (figure 13(*a*)) and up to 50 μm (figure 13(*a*)). This clearly indicates that cracking is not only a concern for the integrity of the solid surface but also a source of dust particles which can be released from the surface.

5. Discussion

The development of the pulsed plasma source on Pilot-PSI is aimed at studying the possibility of synergistic effects caused by the simultaneous exposure of a metallic surface to a divertor-relevant high flux plasma and a transient heat/particle source. Under such conditions, strong release of tungsten is observed at energy densities lower than the energy density for which mass loss is observed in plasma gun experiments, and lower than the energy density at which tungsten emission is observed in the absence of plasma-induced surface modifications [20]. In addition, surface roughening of a tungsten surface is already observed after exposure to 68 s of steady-state plasma and 17 plasma pulses with energy densities as low as 0.07 MJ m^{-2}.

It was observed in [6] that the laser ablation threshold of tungsten was strongly reduced by the formation of helium-induced nanostructure on the surface. In the case of a tungsten surface exposed for 5400 s to low energy helium ions, the threshold for tungsten release is lowered to a value of about 12 MW m^{-2} s$^{1/2}$. In that case, the laser pulse duration was about 5–7 ns. Similar observations were made with sub-ms laser pulse duration [19, 20], which is closer to the plasma pulse duration in this study. The tungsten emission from a tungsten surface pre-irradiated by a helium plasma was found to occur at lower energy densities and also found much higher than for a virgin tungsten surface. A lowering of the damage threshold of tungsten was also observed for simultaneous hydrogen plasma and laser exposure in PISCES-A [7]. This effect did not occur when the surface temperature was about 630 °C, underlining the role of the near-surface gas content and voids/bubbles. In both cases, the bursting of holes and blisters containing gas is proposed as a possible explanation for the observed reduced damage threshold. In the experiments described here, the surface temperature for both the helium and hydrogen plasma cases is in a range where such an effect might be expected. The threshold for tungsten release is observed to be as low as 7 MW m^{-2} s$^{1/2}$ for a steady-state plasma exposure time which is 2 orders of magnitude lower than the duration of the plasma pre-irradiation period in [6]. It is not possible to precisely assess at present where this dramatic difference comes from. However, those results strongly suggest that in the case of a combined exposure to a high flux plasma and a transient heat/particle source, the role of synergistic effects on the surface damage is strongly enhanced.

In addition to a reduced threshold for tungsten release, strong modifications of tungsten surfaces have been observed for energy densities as low as 0.07 MJ m^{-2} and only 17 pulses. Similar surface roughening of tungsten has been observed in [21] for tungsten exposed to the JUDITH electron gun where a tungsten surface is bombarded by high energy electrons. This is attributed to the plastic deformation of the heated grains due to compressive stresses during the transient heating which leads to irreversible swelling after the cool-down [21]. Such an effect is observed when the base temperature of the material is already above the ductile to brittle transition temperature (DBTT) [22] which is clearly the case in the present experiments. In [21], the energy density at which surface roughening is observed depends on the material grade and preparation but even in the worst case is around 0.2 MJ m^{-2} which is much higher than the energy density at which surface roughening is observed in the present experiments where the sample is exposed to the transient heat/particle pulse while being exposed to a hydrogen plasma. This again suggests that the damage of tungsten is enhanced under the specific experimental conditions of the pulsed plasma source system in Pilot-PSI, which simulate the conditions expected during ELMs in ITER.

6. Conclusions

Pulsed operations of the Pilot-PSI plasma source enable ELM simulation experiments with relevant steady-state plasma conditions and transient heat/particle source, allowing plasma–surface interactions under those conditions to be studied in a self-consistent manner. Energy densities as high as 1 MJ m^{-2} have been reached for a pulse duration of 1 ms, in a variety of gases (H, He, Ar). First experiments were made to investigate the effect of the combined steady-state/pulsed plasma on the morphology of polycrystalline tungsten targets. Tungsten release during the plasma pulse was monitored with a fast visible camera filtered around the W I line at 400.9 nm. A clear threshold behaviour is observed. In the case of a hydrogen plasma, the threshold for release is around 0.2 MJ m^{-2}, while no release is observed below 0.25 MJ m^{-2} for helium. Significant morphology changes are observed when the surface is exposed to combined steady-state/pulsed plasmas. Surface roughening is already noticeable after 10 pulses at 0.07 MJ m^{-2}, and increases with the number of pulses. Our results strongly suggest that in the case of a combined exposure to a high flux plasma and a transient heat/particle source, the role of synergistic effects on the surface damage is strongly enhanced.

Acknowledgments

The authors gratefully acknowledge the help and support from the Pilot-PSI staff. This work is part of the research programme of the Stichting voor Fundamenteel Onderzoek der Materie (FOM), which is financially supported by the Nederlandse Organisatie voor Wetenschappelijk Onderzoek (NWO). It is supported by the European Communities under the contract of Association between EURATOM and FOM and carried out within the framework of the European Fusion Programme.

References

[1] Klimov N. *et al* 2009 *J. Nucl. Mater* **390–391** 721
[2] Pitts R.A., Kukushkin A., Loarte A., Martin A., Merola M., Kessel C.E., Komarov v. and Shimada M. 2009 *Phys. Scr.* **T138** 014001
[3] Loarte A. *et al* 2007 *Phys. Scr.* **T128** 222
[4] Tokunaga K., Baldwin M.J., Doerner R.P., Noda N., Kubota Y., Yoshida N., Sogabe T., Kato T. and Schedler B. 2005 *J. Nucl. Mater.* **337–339** 887
[5] Kajita S., Sakaguchi W., Ohno N., Yoshida N. and Saeki T. 2009 *Nucl. Fusion* **49** 095005
[6] Kajita S.,Ohno N., Takamura S., Sakaguchi W. and Nishijima D. 2007 *Appl. Phys. Lett.* **91** 261501
[7] Umstadter K.R., Doerner R. and Tynan G. 2009 *Phys. Scr.* **T138** 014047
[8] Hirai T. *et al* 2007 *Phys. Scr.* **T128** 166
[9] Garkusha I.E., Arkhipov N.I., Klimov N.S., Makhlaj V.A., Safronov V.M., Landman I. and Tereshin V.I. 2009 *Phys. Scr.* **T138** 014054
[10] De Temmerman G., Zielinski J.J., van der Meiden H., Melissen W. and Rapp J. 2010 *Appl. Phys. Lett.* **97** 081502
[11] Zielinski J.J., Al R., van der Meiden H., Melissen W., Rapp J. and De Temmerman G. 2010 *J. Nucl. Mater.* at press doi:10.1016/j.jnucmat.2010.10.023
[12] van Rooij G.J. *et al* 2007 *Appl. Phys. Lett.* **90** 121501
[13] van der Meiden H.J. *et al* 2008 *Rev. Sci. Instrum.* **79** 013505
[14] Herrmann A., Junker W., Gunther K., Bosch S., Kaufmann M., Neuhauser J., Pautasso G., Richter Th. and Schneider T. 1995 *Plasma Phys. Control. Fusion* **37** 17
[15] Hermann A. and ASDEX-Upgrade team 2001 Limitations for divertor heat flux calculations of fast events in tokamaks *Contribution to the 27th Conf. on Plasma Physics and Controlled Fusion (Budapest, Hungary, 12–16 June 2000)*
[16] Eich T., Andrew P., Herrmann A., Fundamenski W., Loarte A., Pitts R.A. and JET-EFDA contributors 2007 *Plasma Phys. Control. Fusion* **49** 573
[17] De Temmerman G., Delchambre E., Dowling J., Kirk A., Lisgo S. and Tamain P. 2010 *Plasma Phys. Control. Fusion* **52** 095005
[18] De Temmerman G., Bacharis M., Dowling J. and Lisgo S. 2010 *Nucl. Fusion* **50** 105012
[19] Kajita S., Takamura S., Ohno N., Nishijima D., Iwakiri H. and Yoshida N. 2007 *Nucl. Fusion* **47** 1358
[20] Kajita S., Ohno N., Sakaguchi W. and Takagi M. 2009 *Plasma Fusion Res.* **4** 1
[21] Linke J. *et al* 2010 in Fusion Energy *(Proc. 23rd Int. Conf. Daejeon) (Daejeon, Korea, October 2010)* (Vienna: IAEA) CD-ROM file EXD/P3-21 http://www-pub.iaea.org/mtcd/meetings/cn180_papers.asp
[22] Callister W.D. Jr 2000 *Materials Science and Engineering: an Introduction* (New York: Wiley)